New Journal of Physics
The open-access journal for physics

Attosecond pulse generation from aligned molecules—dynamics and propagation in H_2^+

E Lorin[1,3], **S Chelkowski**[2] **and A D Bandrauk**[1,2]

[1] Centre de Recherches Mathématiques, Montréal, QC, H3T 1J4, Canada
[2] Laboratoire de chimie théorique Faculté des Sciences, Université de Sherbrooke, QC, J1K 2R1, Canada.
E-mail: Emmanuel.Lorin@uoit.ca

New Journal of Physics **10** (2008) 025033 (21pp)
Received 17 September 2007
Published 29 February 2008
Online at http://www.njp.org/
doi:10.1088/1367-2630/10/2/025033

Abstract. The dynamics and propagation effects in attosecond (asec) pulse generation from high-order harmonic generation (HHG) of aligned one-dimensional (1D) H_2^+ molecules are investigated from numerical solutions of fully coupled Maxwell and time-dependent Schrödinger equations (Maxwell-TDSEs), in the highly nonlinear nonperturbative regime of laser–molecule interaction. Density, laser-phase and propagation length effects are studied on the total electric field and nonlinear polarization from the Maxwell-TDSE for intense few cycle (800 nm) laser pulses interacting with a 1D H_2^+ gas. We show how single and double asec pulses can be generated and propagated as a function of the phase of individual harmonics created by ultrashort intense laser pulses in aligned H_2^+ molecules. We find furthermore extension of maximum HHG plateaux with increasing gas pressure.

[3] Present address: Faculty of Science, University of Ontario Institute of Technology, 2000 Simcoe Street North, Oshawa, ON, L1H 7Y4, Canada.

Contents

1. Introduction

High-order harmonic generation (HHG) in atomic gases by high intensity ultrashort laser pulses is the main method for producing coherent extreme ultraviolet and attosecond (asec) pulses [1]. This is based on a universal model of electron-recollision with a maximum harmonic energy,

$$N\hbar\omega = I_p + 3.17U_p, \tag{1}$$

where I_p is the ionization potential of the atom, $U_p = e^2E^2/4m\omega^2$ is the ponderomotive energy of the electron in an oscillatory field $E(t)$ of maximum intensity $I = eE^2/8\pi$ and frequency ω [2]–[7]. Molecules offer an interesting new medium as both ionization and recombination steps are dependent on the particular symmetry of the highest occupied molecular orbital (HOMO) and orientation [5]–[8]. Furthermore, at large distances, stretched or dissociated molecules offer the possibility of obtaining harmonics well beyond the $3U_p$ cut-off law (1) [5, 9, 10]. The recombination model allows a full tomographic reconstruction of the HOMO to be performed (but a high degree of spatial alignment of the molecules is required [11]–[13]). The mathematical steps in structural retrieval from HHG are based upon the strong field approximation (SFA), a single active electron model and a three-step process [2, 3]: (i) tunneling ionization with zero initial electron velocity; (ii) acceleration in the laser field $E(t)$; and (iii) recombination back into the bound electronic state. This simple three-step model can be shown to always produce a maximum return energy given by (1) even with nonzero initial velocity upon ionization [4]. Nevertheless certain important issues remain, such as the influence of the intense laser field upon the bound electronic states upon recombination [14], depletion of the initial ground state [15], the influence of the Coulomb potential upon the continuum electron states [16], all effects neglected in SFA. Finally, one needs to consider macroscopic propagation effects as these lead to interesting new phenomena such as filamentation [17, 18] with the conclusion that ionization dynamics can strongly influence the synthesis of isolated attosecond pulses [19]. In this paper, we address the problem of asec pulse generation and propagation by HHG in an aligned molecular medium. We focus our attention on the single electron H_2^+ system which nevertheless involves coupled electron–nuclear motion beyond the Born–Oppenheimer approximation [20]. For this H_2^+ system a previous time-dependent Schrödinger equation (TDSE) simulation with exact non-Born–Oppenheimer solutions leads to enhanced ionization and HHG in the presence of an asec XUV and IR fs pulse with the resulting

efficient generation of new asec pulses [21]. An appropriate Maxwell-TDSE equation for this system was used based on a slowly varying envelope approximation (SVEA) leading to a first-order partial differential equation for the coupled Maxwell-TDSE system [22]. Such an approach neglects ground state depletion due to ionization, neglects backward propagation and is therefore appropriate for low field strengths. It was nevertheless found that initial asec pulses could be shortened further in time through the resultant HHG asec pulses produced nonlinearly in the presence of an intense IR fs pulse [23]. In the present paper, we extend the Maxwell-TDSE approach beyond SVEA in order to include the above neglected effects. Particular attention will be given to the harmonic phases to understand more precisely the asec pulse generation.

Section 2 is devoted to the presentation of the Maxwell–Schrödinger model initially introduced in [24, 25]. In section 3, we study the asec pulse generation mechanism using in particular a model describing the transmitted electric field phase. Section 4 is devoted to numerical simulations for the propagation of electric fields and asec pulses inside an aligned H_2^+ gaseous medium. We also present a new phenomenon, a study of the driver phase effect on the HHG and laser pulse propagation.

2. Maxwell-TDSE model

We study the process of asec pulse generation by the analysis of harmonic phases, and their behavior depending on the driver phase, using a model that is a micro–macro Maxwell-TDSE approach [24, 26]. It consists of the coupling of the Maxwell equations and TDSEs within or beyond the Born–Oppenheimer approximation. The model is totally non-perturbative, vectorial and multidimensional, taking into account ionization, and high-order nonlinearities going far beyond classical and semi-classical nonlinear Maxwell and Schrödinger models [25], [27]–[29]. In the present work, we restrict ourselves to 1D TDSEs and 1D propagation in the fixed nuclei approximation (Born–Oppenheimer), for which the equations are:

$$\begin{cases} \partial_t B_x(z',t) = c\partial_{z'} E_y(z',t), \\ \\ \partial_t E_y(z',t) = c\partial_{z'} B_x(z',t) - 4\pi\,\partial_t P_y(z',t), \end{cases} \tag{2}$$

where

$$P_y(z',t) = -n(z') \int \psi_{z'}(y,t)\, y\, \psi^*_{z'}(y,t)\,\mathrm{d}y = -n(z')\, d_{z'}(t). \tag{3}$$

$n(z')$ is the molecular density taken equal to a constant n_0 in the following, $\psi_{z'}$ the wavefunction of a molecule located at z' (the dipole approximation is used here). In the following, we will denote by E the electric field component E_y, and by P the component P_y of the field-induced polarization. In the TDSEs, we suppose that the electric field E is constant in space at the molecular scale $\Delta y/\lambda \ll 1$, so that the electric field in z', $E(z',t)$, is rewritten $E_{z'}(t)$. Alternatively one can use the acceleration of the electron as given in [14] (Fourier transform $\hat{a}(\omega) = \omega^2 d(\omega)$).

$$a(z',t) = \int \psi_{z'}(y,t)\Big(-\frac{\partial V(y,R_0)}{\partial y} + E(t)\Big)\psi^*_{z'}(y,t)\,\mathrm{d}y. \tag{4}$$

In the 1D framework, we can then rewrite equations (3) and (4) as the second-order wave equation

$$\partial^2_{tt} E(z',t) - c^2 \partial^2_{z'z'} E(z',t) = -4\pi\,\partial^2_{tt} P(t). \tag{5}$$

The 1D electron wavefunction is solved by the following TDSE:

$$\mathrm{i}\partial_t \psi_{z'}(y,t) = \left(-\frac{\Delta}{2} + V_c(y, R_0) + yE_{z'}(t)\right)\psi_{z'}(y,t). \tag{6}$$

In the previous equation, R_0 denotes the molecular internuclear distance, z' the field propagation coordinate and y the electric field polarization corresponding to the electron coordinate. The field model allows us to consider high-order nonlinearities as well as ionization. The model is solved using a finite difference method described in detail in [24], where a full non-Born–Oppenheimer formulation is also presented. In the model, we solve one TDSE per Maxwell cell, using a classical Crank–Nicolson scheme, corresponding to $n_0\Delta z'$ molecules. Each Maxwell spatial step $\Delta z'$ is chosen such that $\Delta z' < \lambda_{\max}/5$, where $\lambda_{\max}$ is the largest internal wavelength considered in the computation (allowing then to consider high-order harmonics). For details we refer to [24]. This model is then used to study asec pulse generation and propagation in the presence of HHG.

In conclusion, as we solve one single TDSE per Maxwell cell $\Delta z'$, a computation of N TDSEs corresponds to a sample of gas of length $l = N\Delta z'$ and containing $N\Delta z' n_0$ molecules, where the molecular density n_0 is supposed constant.

3. Theoretical study of harmonic phase effects on asec pulse generation

In order to understand the generation and dynamics of asec pulses, we propose a model to approximate harmonic spectrum extrema. More precisely, we propose to approximate by a continuous function the maxima and minima of the harmonic spectrum and to isolate one or two asec pulses by Fourier transform filtering of these extrema. We then plan to model the frequency-dependent harmonic phase function $\phi(\omega) = \arctan(\mathrm{Im}(\hat{a}(\omega))/\mathrm{Re}(\hat{a}(\omega))$ of the acceleration $\hat{a}(\omega) = |\hat{a}(\omega)|\exp(\mathrm{i}\phi(\omega))$, where $\hat{a}(\omega)$ is the Fourier transform of $a(t)$ defined in (4). This will be done near the cut-off frequency (a few-cycle laser pulse with $I \sim 10^{15}\,\mathrm{W\,cm^{-2}}$).

The simplest model to approximate the dipole acceleration phase of $a(t)$ (4) consists of introducing the following function f_{M}, modeling a spectral maximum around $\omega = 0$ with a piecewise constant phase:

$$f_{\mathrm{M}}(\omega) = -\exp(-\alpha_1\omega)\exp(\mathrm{i}\phi_1)\mathbf{1}_{\mathbb{R}_-}(\omega) - \exp(\alpha_2\omega)\exp(\mathrm{i}\phi_2)\mathbf{1}_{\mathbb{R}_+}(\omega). \tag{7}$$

The constant coefficient ϕ_1 corresponds to the left-phase (phase on the left of a maximum) and ϕ_2 corresponds to the right-phase (phase on the right of a maximum). Coefficients α_1 and α_2, assumed strictly positive, allow in particular to control the harmonic width. Finally, the function $\mathbf{1}_{\mathbb{R}_-}$ is defined as 1 for negative ωs and 0 for positive ones, and $\mathbf{1}_{\mathbb{R}_+}(\omega)$ denotes the function equal to 1 for positive ωs and 0 for negative ones (Heaviside functions).

To model a spectral minimum, we consider f_{m} with a piecewise constant phase:

$$f_{\mathrm{m}}(\omega) = -\exp(\alpha_1\omega)\exp(\mathrm{i}\phi_1)\mathbf{1}_{\mathbb{R}_-}(\omega) - \exp(-\alpha_2\omega)\exp(\mathrm{i}\phi_2)\mathbf{1}_{\mathbb{R}_+}(\omega). \tag{8}$$

We next compute the Fourier transform of f_{M} and f_{m} in order to determine if one or two asec pulses are created. Our goal is therefore to determine for which condition $(\phi_1, \phi_2, \alpha_1, \alpha_2)$ one single asec pulse can be isolated.

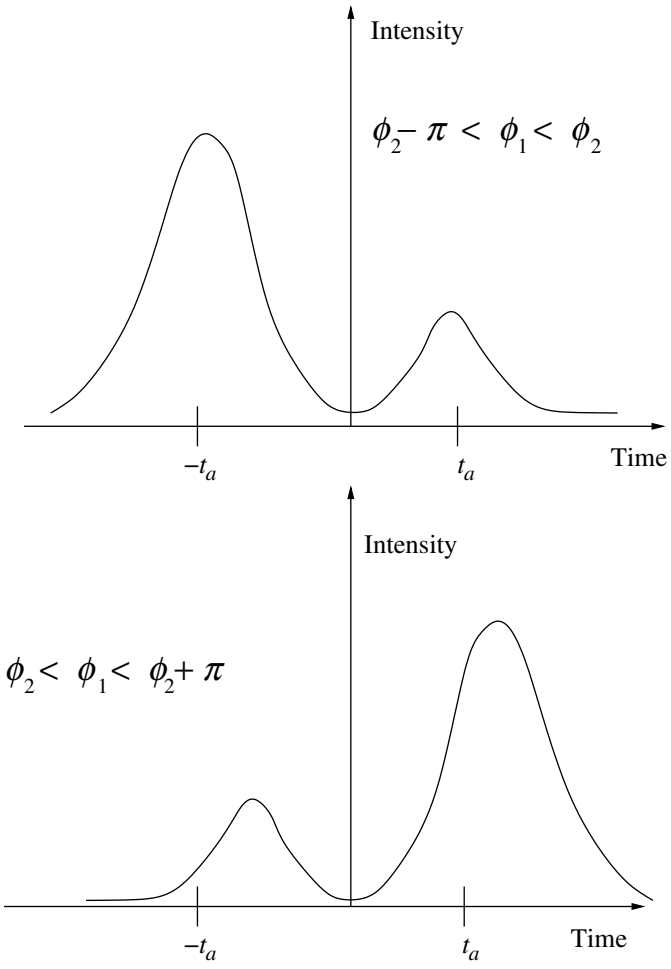

Figure 1. Harmonic phases ϕ_1 and ϕ_2 emitted at times $-t_a$, t_a producing nonsymmetric asec pulses (equation (13)).

From (7) and (8), we next prove the following:

1. If $\phi_1 \neq \phi_2 + k\pi$ ($k \in \mathbb{Z}$, where $\mathbb{Z}$ is the set of negative and positive integers) two non-symmetric asec pulses are created. If $\phi_1 = \phi_2$, there exists one single asec pulse and two symmetric asec pulses if $\phi_1 = \phi_2 + \pi$. Moreover, the asec pulse time durations are proportional to $1/\alpha_1$ and $1/\alpha_2$.
2. For two HHG emitted at times t_a and $-t_a$, then two situations occur depending on the phases ϕ_1 and ϕ_2.

When two non-symmetric asec pulses are created we can identify if the more intense asec pulse is created before or after the less intense one according to figure 1.
First, we examine the Fourier transform of f_{M} which gives a_{M}:

$$a_{\mathrm{M}}(t) = \frac{(\alpha_2 - \mathrm{i}t)\exp(\mathrm{i}\phi_1) + (\alpha_1 + \mathrm{i}t)\exp(\mathrm{i}\phi_2)}{(\alpha_1 + \mathrm{i}t)(\alpha_2 - \mathrm{i}t)}, \tag{9}$$

and

$$\begin{cases} |a_{\mathrm{M}}(t)|^2 = \dfrac{at^2+bt+c}{(\alpha_1^2+t^2)(\alpha_2^2+t^2)}, \\ a = 2(1-\cos(\phi_1-\phi_2)), \\ b = 2(\alpha_1+\alpha_2)\sin(\phi_1-\phi_2), \\ c = 2\alpha_1\alpha_2\cos(\phi_1-\phi_2)+\alpha_1^2+\alpha_2^2. \end{cases} \tag{10}$$

The function $|a_{\mathrm{M}}(t)|^2$ is naturally symmetric if and only if $b=0$, i.e. $\phi_1=\phi_2+k\pi$, $k\in\mathbb{Z}$. In the opposite case, we can directly conclude that this function is not symmetric, so that two pulses are created. Now, if $\phi_1=\phi_2$, we observe that $|a(t)|^2$ degenerates into:

$$|a_{\mathrm{M}}(t)|^2 = \frac{(\alpha_1+\alpha_2)^2}{(\alpha_1^2+t^2)(\alpha_2^2+t^2)}. \tag{11}$$

This allows us to conclude that one *single* asec pulse is created. If $\phi_1=\phi_2+\pi$, then

$$|a_{\mathrm{M}}(t)|^2 = \frac{4t^2+(\alpha_1+\alpha_2)^2}{(\alpha_1^2+t^2)(\alpha_2^2+t^2)}. \tag{12}$$

which gives two symmetric asec pulses.

Classical Fourier analysis allows the conclusion that for small α_1 and α_2 the two asec pulses birth times are very close and naturally far for large α_1 and α_2. Assuming that $\alpha_1=\alpha_2=\alpha>0$, we set $s=t/\alpha$ and $\phi=\phi_1-\phi_2$, then

$$|a(s)|^2 = \frac{(1-\cos(\phi))s^2+\sin(\phi)s+1+\cos(\phi)}{1+s^2}. \tag{13}$$

This then corresponds to the case $\alpha=1$. The distance between the two asec pulse maxima is then proportional to $1/\alpha$ in accordance with statement 1 above.

For the second point, it is sufficient to study the ratio $c:=|a(t_a)|/|a(-t_a)|$. We simply observe that $c>1$ if and only if $b<0$ and only if $\sin(\phi_1-\phi_2)<0$ and only if $\phi_2-\pi<\phi_1<\phi_2$.

This simple analysis allows the transfer of the asec pulse generation conditions on the behavior of the phase of the dipole acceleration spectrum $\hat{a}(\omega)=|\hat{a}(\omega)|\exp(\mathrm{i}\phi(\omega))$. However, it is not sufficiently precise as the behavior of the acceleration harmonic phase is in fact more complex. We then consider a more general maximum defined by:

$$g_{\mathrm{M}}(\omega) = -\left(\mathbf{1}_{\mathbb{R}_-}(\omega)\chi(-\alpha_1,\omega,A)+\mathbf{1}_{\mathbb{R}_+}(\omega)\chi(\alpha_2,\omega,A)\right)\exp(\mathrm{i}\phi(\omega)). \tag{14}$$

χ is a smooth function defined by

$$\chi(\alpha,\omega,A) = \begin{cases} \exp(\alpha\omega)-A, & \text{if } \exp(\alpha\omega)\leqslant A, \\ 0, & \text{otherwise.} \end{cases} \tag{15}$$

We denote by Ω the support of χ (i.e. $\chi(x)=0$ for all $x\in\Omega^c$) and A is a positive real constant related to the depth of the minima. In order to study the asec pulse generation around a minimum we introduce similarly the more general amplitude,

$$g_{\mathrm{m}}(\omega) = -\left(\mathbf{1}_{\mathbb{R}_-}(\omega)\chi(\alpha_1,\omega,A)+\mathbf{1}_{\mathbb{R}_+}(\omega)\chi(-\alpha_2,\omega,A)\right)\exp(\mathrm{i}\phi(\omega)). \tag{16}$$

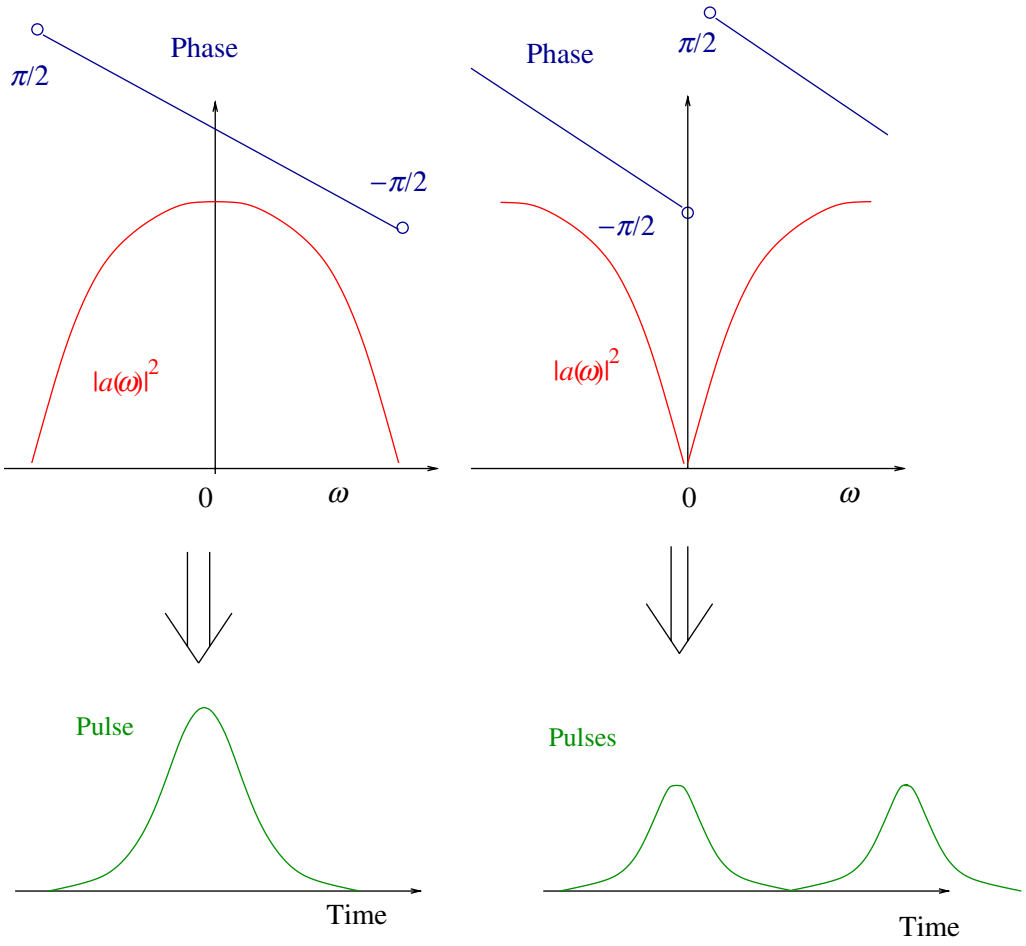

Figure 2. One or two asec pulse generation from maxima and minima in the HHG spectrum depending on the harmonic phase ϕ (equation (12)).

For simplicity, we suppose that the phase is not piecewise constant but rather piecewise linear. This allows us to conclude that:

1. For g_{M} defined in (14) with $\phi(\omega) = -\pi\omega/2$, one single asec pulse is generated.
2. Whereas for g_{m} defined in (16) with $\phi(\omega) = -(\pi/2)(\omega+1)\mathbf{1}_{\mathbb{R}_-}(\omega) - (\pi/2)(\omega+1)\mathbf{1}_{\mathbb{R}_-}(\omega)$, then two symmetric asec pulses are created.

To prove this, it is sufficient to observe that setting $t' = t - \pi/2$, we recover the case $\phi(\omega) = 0$ studied above leading to one single attosecond pulse generation. The second case can be proven in the same manner. It is sufficient to observe that setting $t' = t + \pi/2$, we recover the case $\phi(\omega) = -\pi/2$ for negative ω and $\phi(\omega) = \pi/2$ for positive ones, leading to two attosecond pulses being generated. This is illustrated and summarized in figure 2.

In general, we can observe periodic behavior of the acceleration harmonic phase $\phi(\omega) = \arctan(\mathrm{Im}(\hat{a}(\omega))/\mathrm{Re}(\hat{a}(\omega)))$. The period is often observed to be numerically equal to $2\omega_{\mathrm{l}}$, with ω_{l} the frequency of the incident laser pulse. We then consider the following phase (where $\mathbb{Z}$ is

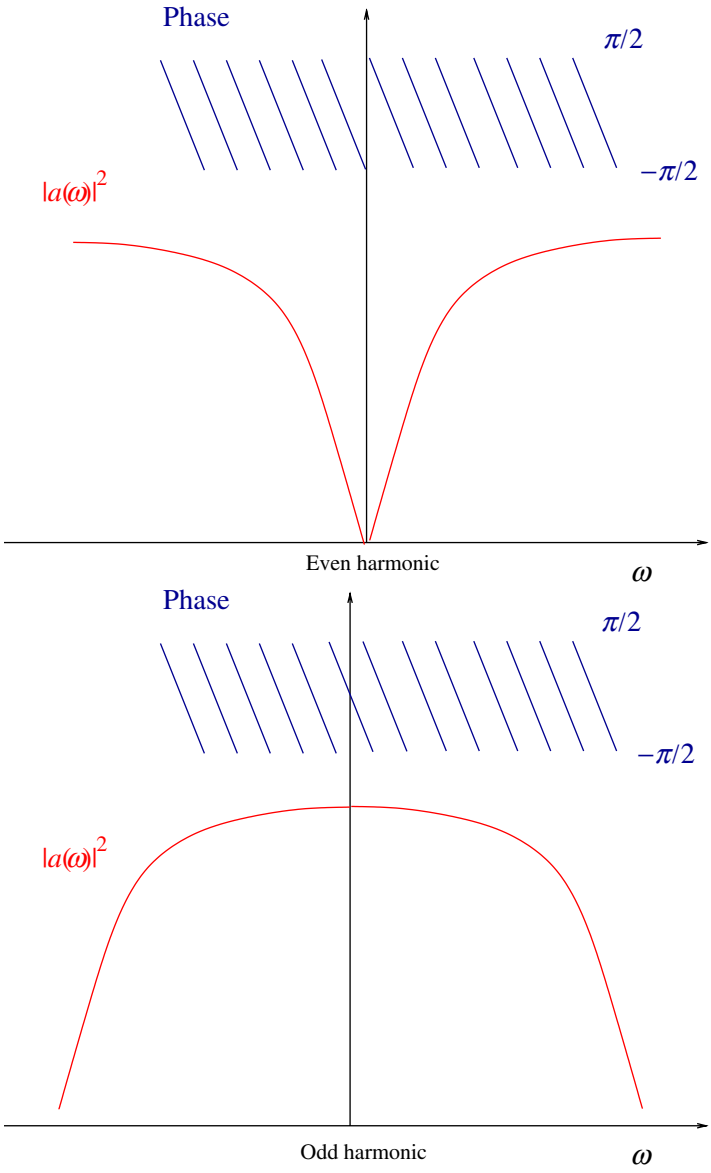

Figure 3. Mathematical modeling of a minimum and a maximum in continuum HHG spectrum $|a(\omega)|^2$ with phases of each harmonic.

the set of negative and positive integers):

$$\phi(\omega) = \sum_{k\in 2\mathbb{Z}} \frac{\pi}{2}(k-\omega)\mathbf{1}_{[k-1,k+1[}(\omega). \tag{17}$$

Note that $\phi(\omega)$ jumps from $-\pi/2$ to $\pi/2$ are due to $\mathrm{Re}(\hat{a}(\omega))$ cancellations (from positive to zero, to negative values). We then consider the following phase function (see figure 3). We consider g_{M} at maxima and g_{m} at minima defined in (14) and (16) with a phase given by (17). We suppose for the sake of simplicity that $\alpha_1 = \alpha_2 = \alpha > 0$. Then one obtains from (14) at a maximum harmonic and for a large enough or small enough α, that *only one single asec pulse is created*. From (16) at a minimum and for large enough or small enough α, two asec pulses

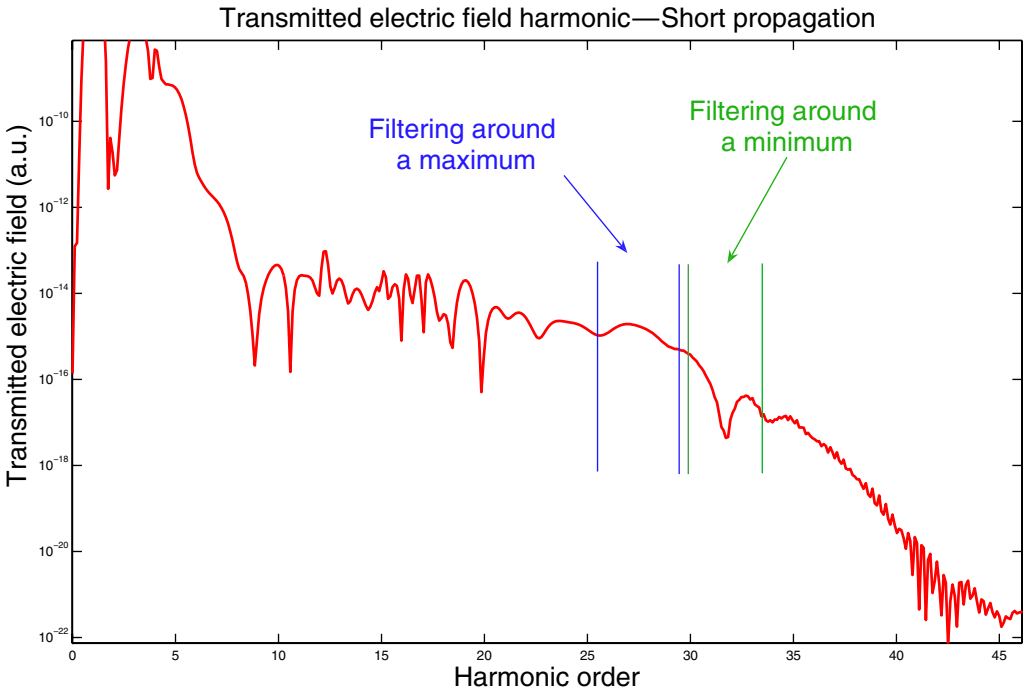

Figure 4. Harmonic spectrum filtering around a maximum and a minimum for 2-cycle 800 nm, $I = 10^{14}\,\mathrm{W\,cm^{-2}}$ pulse with 5 nm propagation length l and density $n = 10^{20}\,\mathrm{mol\,cm^{-3}}$.

are generated. For both minima and maxima the above conclusions follow from application of Fourier transforms as proved further in the appendix.

These results allow us to deduce when one or two asec pulses will be created by analysis of HHG spectra and their phases. We now give an illustration of these analytic results in figures 4 and 5. The example we propose corresponds to the propagation over a very short distance ($\sim$100 au $\sim$ 5 nm) of a 2-cycle laser pulse at 800 nm in a dense medium ($\sim 10^{20}\,\mathrm{mol\,cm^{-3}}$) at intensity $10^{14}\,\mathrm{W\,cm^{-2}}$. We then filter around a minimum (32th harmonic), and a maximum (27th harmonic), figure 4, the transmitted electric field HHG spectrum. As expected, respectively one and two asec pulses (figure 5) are created. The pulse duration is obviously proportional to the filtering range ($\sim$400 as in the example). This study allows us to develop precise conditions to generate one or two asec pulses.

4. HHG and asec pulse propagation

In this section, we examine propagation effects on asec pulse generation studied in section 3 and the harmonic intensities. We then consider the interaction of an aligned 1D H_2^+ molecule gas with intense ultrashort laser pulses. We will also present a new propagation effect at high intensity and density including discussion of driver phase effects.

4.1. Harmonic dynamics and asec pulse propagation

We study here the dynamics of 5-cycle Ti:S laser pulse at 800 nm inside a 1D aligned H_2^+-gas of molecular density $3.5 \times 10^{18}\,\mathrm{mol\,cm^{-3}}$. The intensity of the laser is $10^{14}\,\mathrm{W\,cm^{-2}}$ and the

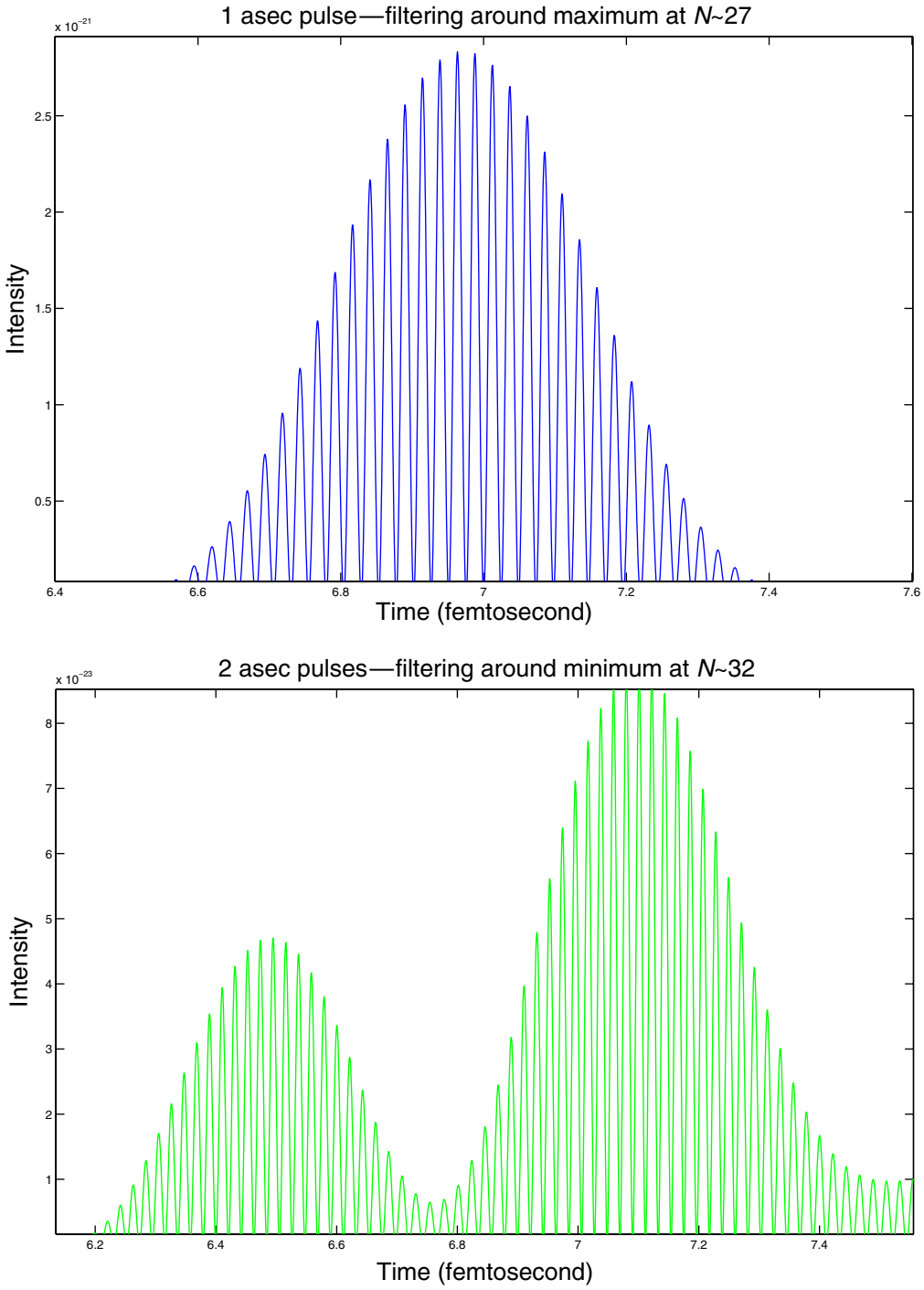

Figure 5. One and two asec pulse generation, with $I = 10^{14}\,\mathrm{W\,cm^{-2}}$, $n_0 = 10^{20}\,\mathrm{mol\,cm^{-3}}$ and propagation length $l = 5\,\mathrm{nm}$ (2-cycle pulse 800 nm).

internuclear distance is fixed (Born–Oppenheimer) at $R_0 = 3.2$ au. Simulations are here 1D and the size of a Maxwell cell is equal to $\Delta z' = 140$ au ~ 7.4 nm.

Of particular interest here is the intensity of the first low harmonics and in the cut-off regime. From the Fourier transform of the transmitted electric field $E_{z'}(t)$ (see (3), (5) and (6)) propagating in the gas at different lengths, we study the evolution of the first (up to 11) harmonic intensities. The harmonic spectrum of the transmitted field, denoted by $\mathbf{E}_T$, possesses, in theory [18], a cut-off frequency given in (1) for recollision of the electron with the parent ion. Collisions with neighboring ions such as in molecules produce larger orders N, due to large collision energies exceeding $3.17U_p$ [4]. We then investigate the harmonic intensities of the transmitted electric field $(\omega, |E_T(\omega)|^2)$ for $N = 3, 7$ and 11 at different distances. We observe that as physically expected, the quadratic scaling (see figure 6) function of the propagation distance (or molecular density) is well respected for small propagation distances. However, after a sufficiently large propagation, nonlinear propagation effects appear (see in particular the 7th and 11th harmonics). In particular, we can observe in figure 7(a) that the 3rd harmonic increases, then is absorbed after a sufficiently large propagation due to the fact that the internuclear distance has been fixed to 3.2 au leading to a 3-photon resonance. These results are comparable with previous atomic calculations [20, 30] (note that a 7-photon resonance also occurs when $R_0 = 2$ au).

We then define the total amount of energy of a selected asec pulse by:

$$\mathbf{E}_c = \int |E_c(t)|^2 \, dt, \qquad \text{with } E_c(t) = \frac{1}{2\pi} \int_{\omega_c - \Delta\omega}^{\omega_c + \Delta\omega} e^{-i\omega t} \hat{E}_T(\omega) \, d\omega, \tag{18}$$

where ω_c is the cut-off frequency and $[\omega_c - \Delta\omega, \omega_c + \Delta\omega]$ the selected frequency range, to isolate one asec pulse as described in section 3. As an example, we analyze a filtered (with $\Delta\omega = 2$, $\omega_c = 33$) asec pulse (time duration $\sim$280 as) propagating over a distance of $l \sim 40\,\mu$m. We compute in figure 7(b) its total amount of energy $\mathbf{E}_c$ (18) (function of the propagation distance) for which oscillating behavior appears. This result is to be compared to results of [22] where a much larger propagation distance is considered but however with a much simpler model, and where the polarization was deduced from one single atom response.

4.2. CEP dependence of HHG

We focus in this section on the effect of the incident laser pulse CEP, i.e. the carrier envelope phase, or laser driver phase ϕ on the harmonic dynamics and consequently on the asec generation. We are especially interested in the dipole acceleration (4) and transmitted electric field harmonic spectra but also in the classical electronic motion. As is well known, a simple classical model allows some very precise information on the electron classical behavior to be obtained, especially in the cut-off frequency of the harmonic spectra (1) [2]–[4]. First, we will introduce a classical model to describe the electron motion. Using this model, we will first explain a phenomenon usually observed on harmonic spectra and asec pulse creation. Then, we will study the harmonic spectra depending on the driver phase ϕ illustrating a new physical phenomenon.

4.2.1. Classical recollision. Let us introduce the following Gaussian electric pulse:

$$E(\omega, t) = E_0 \cos(\omega t + \phi) \exp(-(t - t_0)^2). \tag{19}$$

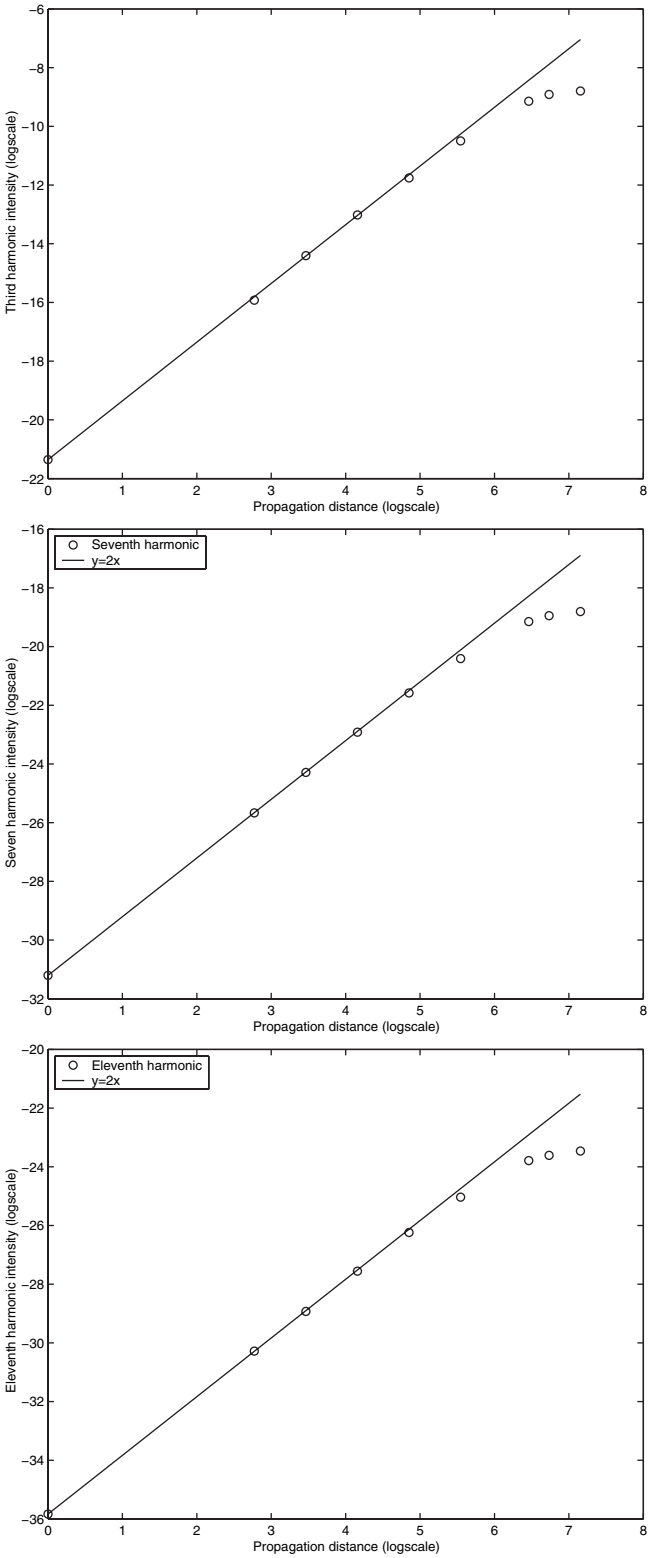

Figure 6. 3rd, 7th and 11th harmonic intensities (logscale), as function of propagation length l, up to 11 μm, for $R_0 = 3.2$ au for 5-cycle 800 nm pulse ($I = 10^{14}\,\mathrm{W\,cm^{-2}}$, $n = 3.5 \times 10^{18}\,\mathrm{mol\,cm^{-3}}$).

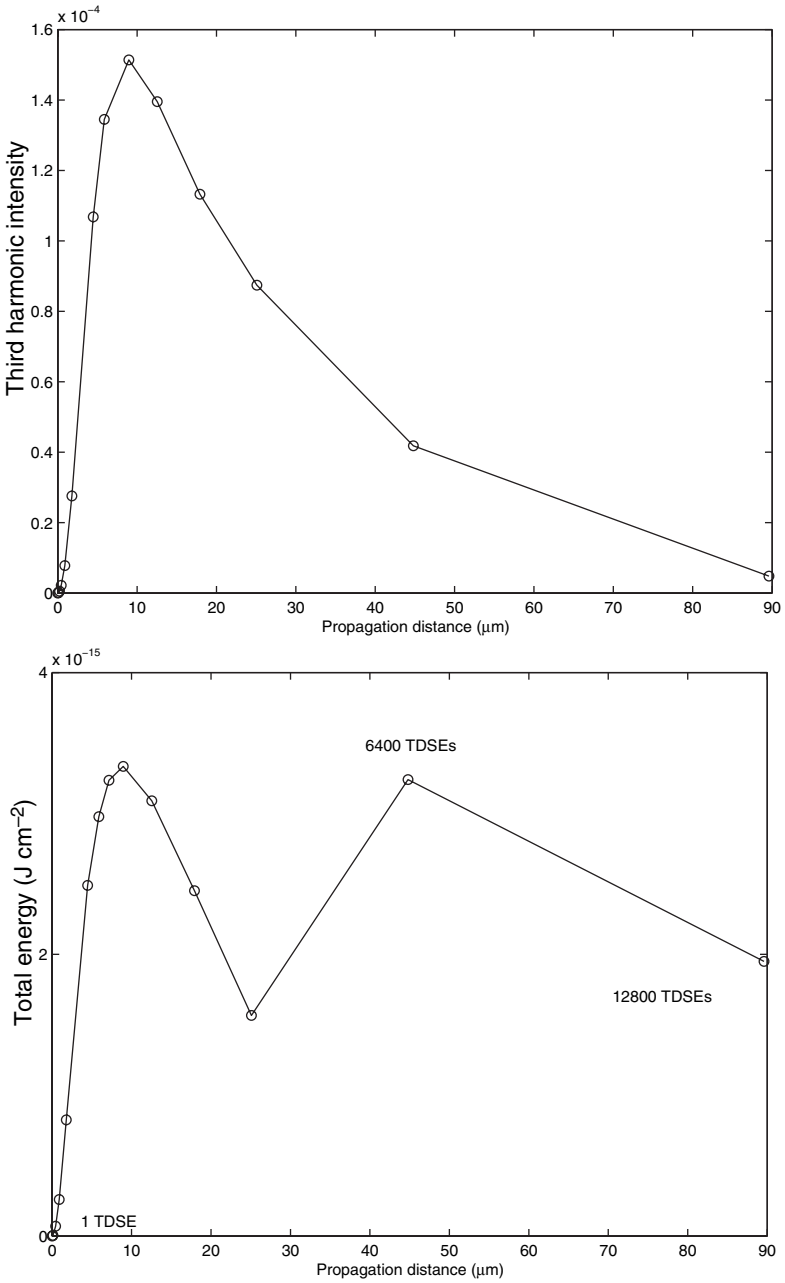

Figure 7. (a) 3rd harmonic absorption (logscale) as function of propagation length l, for $R_0 = 3.2$ au. (b) total energy in the filtered asec pulse depending on the propagation length (up to 90 μm) (harmonic range [25, 35]).

We present different return energy graphs, maxima of energy depending on the driver phase ϕ. The analysis consists of solving Newton's equations for one electron (in au): $\ddot{z}(t) = -E(\omega, t), z(t_0) = z_0, \dot{z}(t_0) = v_0$ from which are deduced the electronic trajectories and the electronic return energy at time t_f depending on ϕ [4]. We propose this simple analysis to explain why near the cut-off frequency, two trajectories separated by $\sim$0.2 cycle are often observed numerically in quantum calculations [14, 31]. To our knowledge, no rigorous explanation has

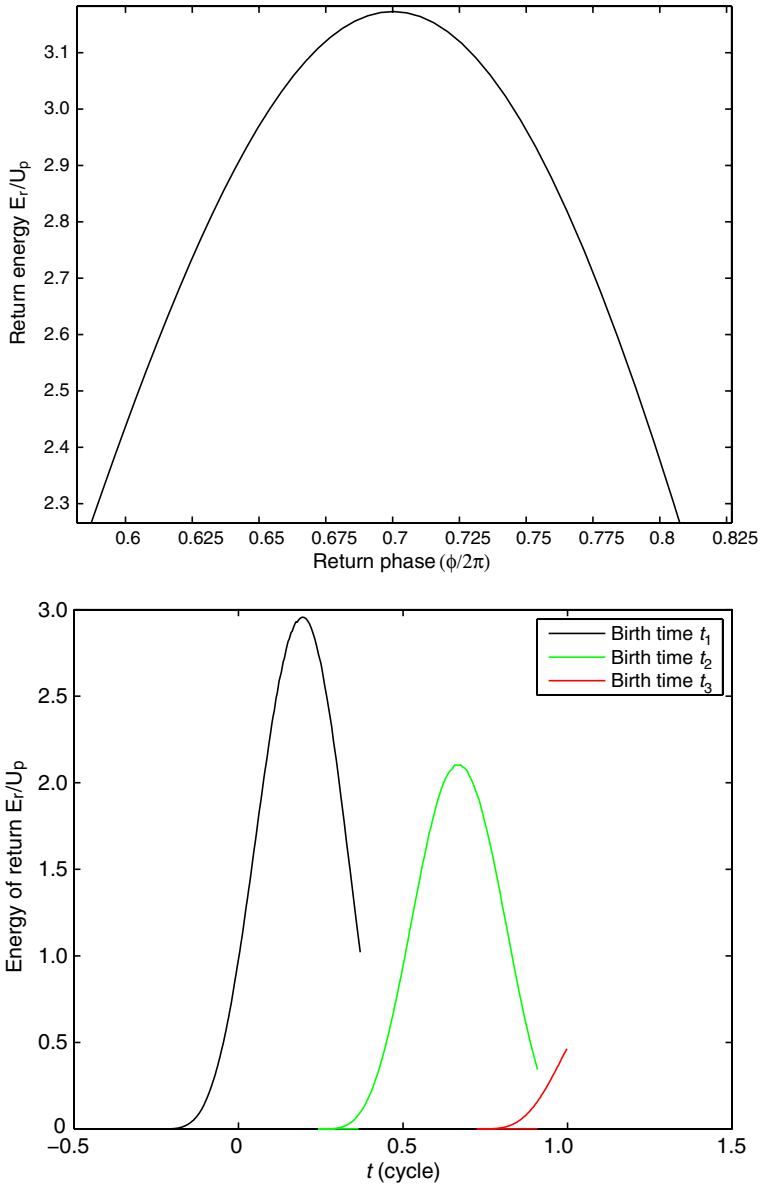

Figure 8. (a) Return energy E_r/U_p (U_p ponderomotive energy) dependence on the phase ϕ_f of return ($\phi_f/2\pi$) for a monochromatic incident pulse $E(t)$. (b) Return energy $E(t)$, equation (19) for $\phi = 0$ and three different birth times t_i.

been provided for this specific phenomenon. For the special case of monochromatic electric fields the energy of return (function of time) is represented in figure 8(a), as obtained from the exact solution of Newton's equations for initial velocity v_0, maximum amplitude E_0, initial field phase ϕ_0, return phase ϕ_f and initial electron position z_0 [4]:

$$z(t_f) = \left(v_0 + \frac{E_0}{\omega}\sin(\phi_0)\right)\frac{\phi_f - \phi_0}{\omega} + (\cos(\phi_0) - \cos(\phi_f))\frac{E_0}{\omega^2} + z_0. \tag{20}$$

We can then deduce the time delay between two trajectories; for instance this delay is 0.1 cycle if the return energy E_r is close to $2.95U_p$ (U_p is the ponderomotive energy (1)), see

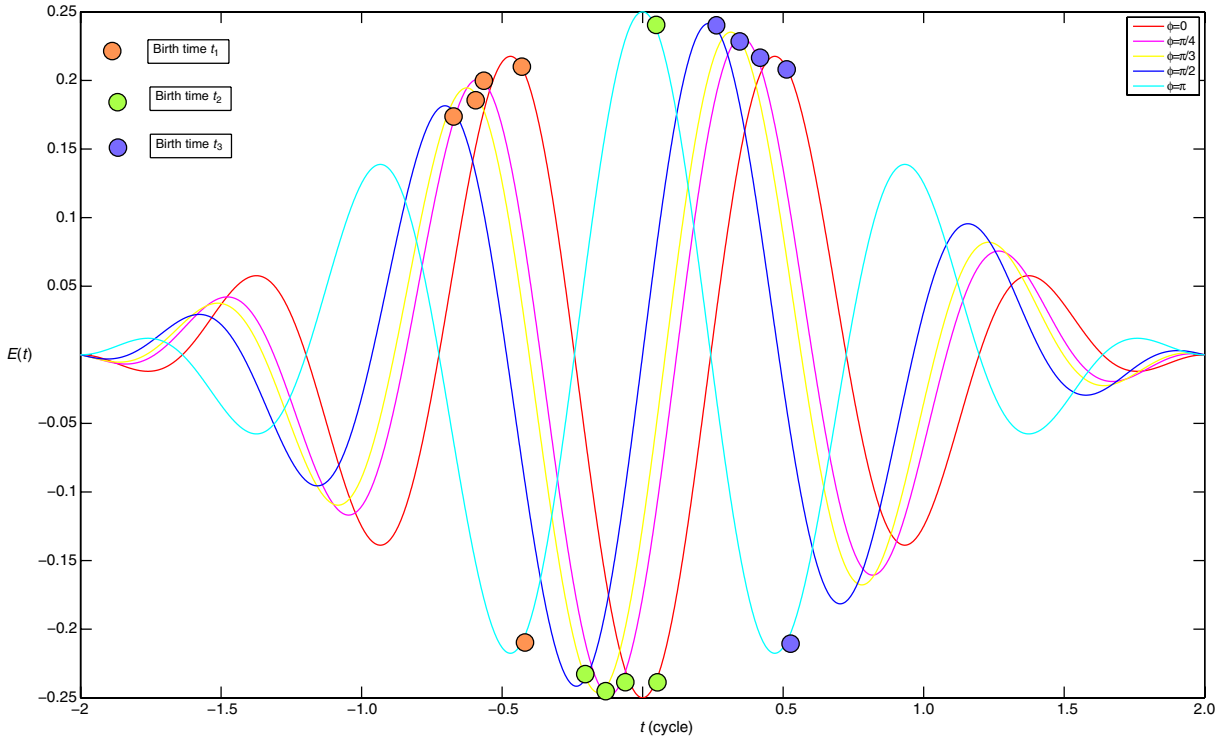

Figure 9. Electric fields $E(t)$ equation (19) with driver phase ϕ and birth times t_i for a four cycle pulse (intensity (in au)/time (in cycles)).

figure 8(a). For shorter pulses, this exact solution is no longer valid as the envelope of the pulse has to be taken into account. We therefore solve numerically Newton's equations for the envelope given by $\exp(-\alpha(t - t_f/2)^2)$ where $\alpha > 0$.

In figures 8(b), we represent the maximum return energy dependence on time (here ϕ is equal to 0, cos pulse) in equation (19), for birth times t_i plotted in figure 9. We recall that $\phi = \pi/2$ (sin pulse) corresponds to the smallest energy, whereas $\phi = 0$ (and $\phi = \pi$) corresponds to the largest one, as is currently observed numerically and experimentally in harmonic spectra. In figure 10, we represent the harmonic spectrum dependence on the phase ϕ [5]. We remark that, as expected, the driver phase $\phi = \pi/2$ gives the shortest cut-off frequency and $\phi = 0$ the longest one in accordance with the classical study presented above.

We finally present results with full propagation of a two- or four-cycle laser pulse within a gas (again represented by many aligned TDSEs via (3) and (6)) and solved by the macroscopic Maxwell's equations (2) with intensities 10^{15} W cm^{-2}. We compute the transmitted electric field harmonics for 1 up to 12 800 TDSEs. These harmonics are obtained from the Fourier transform of the total transmitted field through the gas. In this part, we are especially interested in the harmonic spectra depending on the driver phase.

In figure 11, an interesting new phenomenon has to be noticed when comparing the transmitted electric field $E_{z'}(t)$ (related to many molecules) spectrum with the single molecule dipole harmonics (3). The single molecule dipole spectrum shows deep minima near the cut-off frequency. As we have seen earlier, around these minima two trajectories can often be isolated. By contrast around large continuous maxima (several harmonic orders) one single trajectory returns. We numerically observe that near the cut-off frequency, the deep minima observed in the

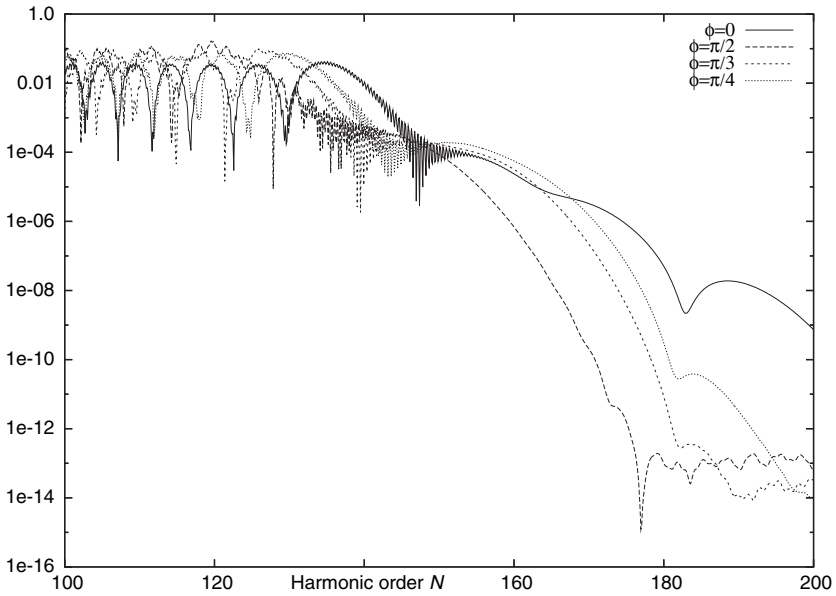

Figure 10. HHG minima dependence on the laser driver phase ϕ.

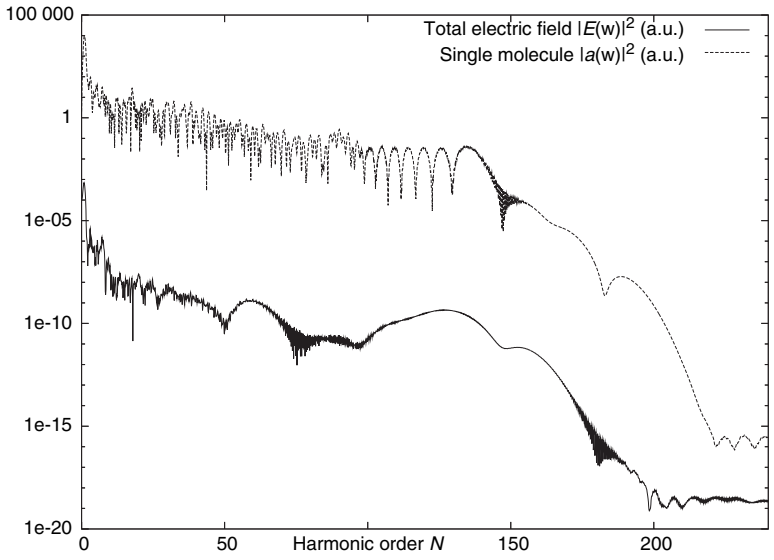

Figure 11. Single molecule dipole acceleration harmonics ($|\hat{a}(\omega)|^2$) and transmitted electric field intensity ($|\hat{E}(\omega)|^2$) (propagation length equal to 10 nm) harmonics. (Deep minima near the cut-off have disappeared after propagation, $I = 10^{15}\,\mathrm{W\,cm^{-2}}$ and $n_0 = 10^{20}\,\mathrm{mol\,cm^{-3}}$, $\phi = 0$.)

dipole acceleration harmonics disappear in the transmitted electric field harmonics (propagation in the gas, less than 1 μm). As a consequence, only one single trajectory seems to 'survive' (see sections 3 and 4.2).

For larger propagation distances and a driver phase equal to 0, figure 12 shows surprising behavior for the 2-cycle pulse. Near the cut-off frequency, the HHG energy is larger than

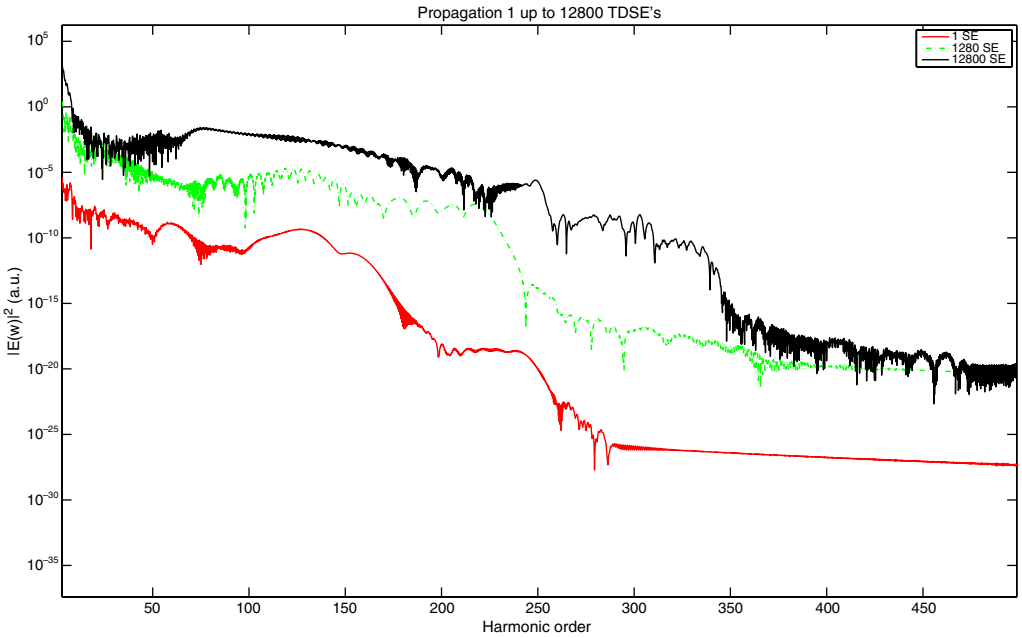

Figure 12. 2-cycle—total electric field harmonic order with propagation for 1, 1280, 12 800 TDSEs corresponding respectively to 7.4 nm, 7.4×1280 nm, $7.4 \times 12\,800$ nm ($I = 10^{15}\,\mathrm{W\,cm^{-2}}$, constant molecular density equal to $n_0 = 10^{20}\,\mathrm{mol\,cm^{-3}}$, 800 nm, $\phi = 0$).

the classical return energy $3.17U_\mathrm{p}(\omega_\mathrm{l}) + I_\mathrm{p}$ after propagation. Furthermore we note the n_0^2 dependence of the efficiency of HHG with propagation, thus confirming it is a coherent collective phenomenon depending on pairs of molecules.

We propose the following explanation for this phenomenon. For large density n_0 and short (2-cycles) and intense ($I = 10^{15}\,\mathrm{W\,cm^{-2}}$) laser pulses a spectral broadening due to Kerr-effect is usually observed [32]. Pulse compression is also operative at high densities (∼1 atm) [17]. We note, however, that our result is opposite to the prediction of cut-off shortening due to non-adiabatic phase matching effects [28]. Therefore, during the propagation spreading occurs to frequencies less than the incident laser frequency ω_l (first harmonic). This produces an increase of the ponderomotive energy U_p ($E_0/4\tilde{\omega}_\mathrm{l}^2$) where $\tilde{\omega}_\mathrm{l} < \omega_\mathrm{l}$. This results in the cut-off increasing with propagation of the laser field in the gas. This phenomenon could be used, we suggest, to produce shorter asec pulses.

5. Conclusion

Ultrashort intense pulse propagation effects on asec pulse generation have been investigated in a 1D Maxwell-TDSE approach for aligned 1D H_2^+ molecules as a function of various parameters: driver pulse phase ϕ, propagation length l and molecule density n_0. The simulations, although limited to the 1D model, take into account field quantum effects, such as ionization, HHG, interference, multiphoton resonance absorption and use a full second-order equation for the propagated field (5).

The first new result as reported in figure 12 is the increase of the HHG cut-off length with increasing molecular density. We propose that this is due to pulse compression effects [17], thus

broadening the spectrum of the driver (incident) pulse with the lower frequencies generated increasing the ponderomotive energy U_p and the maximum cut-off law (1). The second result is the possibility of creating double asec pulses (figure 5) by filtering and recombining harmonics around sharp minima in the HHG spectrum. A detailed theory for the generation of such double asec pulses, their width and temporal separation is presented in section 3 and the appendix. Finally, multiphoton resonance effects are shown to have a limiting effect on total asec pulse energy as a function of propagation lengths (figures 6, 7, etc). Further refinement of these effects are being pursued in a full 3D Maxwell-TDSE treatment using a complete 3D numerical model presented in [24] in order to verify nonlinear absorption effects in propagation of intense pulses in condensed media [33].

Acknowledgments

Funding of this research has been provided by the Centre de Recherches Mathematiques (CRM) and Canada Research Chair (CRC) program. Supercomputer facilities (more than 500 CPUs) were made available by RQCHP. Finally, we acknowledge 'illuminating' discussions with P B Corkum (NRC).

Appendix

To prove the existence of one or two asec pulse generation from HHG, we first begin by applying the Fourier transform to our model equation (14),

$$\mathcal{F}(g_M(t)) = \int_{\mathbb{R}} \exp(i\omega t) g_M(\omega) d\omega = \sum_{\ell \in 2\mathbb{Z}} \int_{\ell-1}^{\ell+1} \exp(i\omega t) g_M(\omega)\, d\omega. \tag{A.1}$$

Now (denoting by $\mathbb{Z}$ the set of negative and positive integers and Ω the support of χ (see section 3))

$$\begin{aligned}
\mathcal{F}(g_M(t)) = & -\sum_{\ell \in 2\mathbb{Z}^*_- \cap \Omega} \int_{\ell-1}^{\ell+1} \exp\left(i\omega(t-\pi/2)\right) \chi(-\alpha, \omega, A) \exp(i\pi\ell/2)\, d\omega \\
& -\sum_{\ell \in 2\mathbb{Z}^*_+ \cap \Omega} \int_{\ell-1}^{\ell+1} \exp\left(i\omega(t-\pi/2)\right) \chi(\alpha, \omega, A) \exp(i\pi\ell/2)\, d\omega \\
& -\int_{-1}^{0} \exp\left(i\omega(t-\pi/2)\right) \chi(-\alpha, \omega, A) \exp(-i\omega\pi/2)\, d\omega \\
& -\int_{0}^{1} \exp\left(i\omega(t-\pi/2)\right) \chi(\alpha, \omega, A) \exp(-i\omega\pi/2)\, d\omega.
\end{aligned} \tag{A.2}$$

If we suppose that α is large enough, the first two terms are negligible compared to the two last as $\chi(\alpha, \omega, A)$ decrease quickly to zero. This then corresponds to the case of a constant phase $\phi_1 = \phi_2 = 0$ studied above and leading to one single asec pulse.

Now as we consider that χ has a compact support (χ is then zero outside a bounded domain) a simple computation leads to (where $\mathbb{Z}^*_-$ are the strictly negative integers and $\mathbb{Z}^*_+$

the strictly positive ones):

$$\begin{aligned}\mathcal{F}(g_{\mathrm{M}}(t)) = & -\sum_{\ell\in 2\mathbb{Z}^*_-\cap\Omega}\exp(\mathrm{i}\ell\pi/2)\frac{\exp\left((\ell+1)(\mathrm{i}t-\mathrm{i}\pi/2-\alpha)\right)-\exp\left((\ell-1)(\mathrm{i}t-\mathrm{i}\pi/2-\alpha)\right)}{\mathrm{i}t-\mathrm{i}\pi/2-\alpha}\\ & -\sum_{\ell\in 2\mathbb{Z}^*_+\cap\Omega}\exp(\mathrm{i}\ell\pi/2)\frac{\exp\left((\ell+1)(\mathrm{i}t-\mathrm{i}\pi/2+\alpha)\right)-\exp\left((\ell-1)(\mathrm{i}t-\mathrm{i}\pi/2+\alpha)\right)}{\mathrm{i}t-\mathrm{i}\pi/2+\alpha}\\ & -\int_{-1}^{0}\exp\left(\mathrm{i}\omega(t-\pi/2)\right)\chi(-\alpha,\omega,A)\exp(-\mathrm{i}\pi/2)\mathrm{d}\omega\\ & -\int_{0}^{1}\exp\left(\mathrm{i}\omega(t-\pi/2)\right)\chi(\alpha,\omega,A)\exp(-\mathrm{i}\pi/2)\mathrm{d}\omega+C(\alpha,A).\end{aligned}\tag{A.3}$$

In the previous formula, $C(\alpha, A)$ (denoted by C in the following) is a real constant that depends on α and A since χ is defined as the sum of an exponential function and a real constant A. If we set $\ell \leftarrow -\ell$ in the first sum on the r.h.s., we obtain:

$$\begin{aligned}\mathcal{F}(g_{\mathrm{M}}(t)) = & -\sum_{\ell\in 2\mathbb{Z}^*_+\cap\Omega}\exp(-\mathrm{i}\ell\pi/2)\\ & \times\frac{\exp\left((-\ell+1)(\mathrm{i}t-\mathrm{i}\pi/2-\alpha)\right)-\exp\left((-\ell-1)(\mathrm{i}t-\mathrm{i}\pi/2-\alpha)\right)}{\mathrm{i}t-\mathrm{i}\pi/2-\alpha}\\ & -\sum_{\ell\in 2\mathbb{Z}^*_+\cap\Omega}\exp(\mathrm{i}\ell\pi/2)\frac{\exp\left((\ell+1)(\mathrm{i}t-\mathrm{i}\pi/2+\alpha)\right)-\exp\left((\ell-1)(\mathrm{i}t-\mathrm{i}\pi/2+\alpha)\right)}{\mathrm{i}t-\mathrm{i}\pi/2+\alpha}\\ & -\left(\frac{1-\exp(\alpha+\mathrm{i}\pi/2-\mathrm{i}t)}{\mathrm{i}t-\alpha-\mathrm{i}\pi/2}+\frac{\exp(\alpha+\mathrm{i}t-\mathrm{i}\pi/2)-1}{\mathrm{i}t+\alpha-\mathrm{i}\pi/2}\right)+C.\end{aligned}\tag{A.4}$$

Note also that $\ell\in 2\mathbb{Z}\cap\Omega$ so that $\exp(\mathrm{i}\ell\pi/2)=\exp(-\mathrm{i}\ell\pi/2)$. In the following, we will denote $\Omega_{2+}=2\mathbb{Z}^*_+\cap\Omega$

$$\begin{aligned}\mathcal{F}(g_{\mathrm{M}}(t)) = & -\sum_{\ell\in\Omega_{2+}}\exp(\mathrm{i}\ell\pi/2)\\ & \times\left(\frac{\exp\left((\ell-1)\alpha\right)\exp\left((\ell-1)(\mathrm{i}\pi/2-\mathrm{i}t)\right)-\exp\left((\ell+1)\alpha\right)\exp\left((\ell+1)(\mathrm{i}\pi/2-\mathrm{i}t)\right)}{\mathrm{i}t-\mathrm{i}\pi/2-\alpha}\right.\\ & \left.+\frac{\exp\left((\ell+1)\alpha\right)\exp\left((\ell+1)(\mathrm{i}t-\mathrm{i}\pi/2)\right)-\exp\left((\ell-1)\alpha\right)\exp\left((\ell-1)(\mathrm{i}t-\mathrm{i}\pi/2)\right)}{\mathrm{i}t-\mathrm{i}\pi/2+\alpha}\right)\\ & -\left(\frac{1-\exp(\alpha+\mathrm{i}\pi/2-\mathrm{i}t)}{\mathrm{i}t-\alpha-\mathrm{i}\pi/2}+\frac{\exp(\alpha+\mathrm{i}t-\mathrm{i}\pi/2)-1}{\mathrm{i}t+\alpha-\mathrm{i}\pi/2}\right)+C.\end{aligned}\tag{A.5}$$

Thus, if we set $B=t-\pi/2$

$$\begin{aligned}\mathcal{F}(g_{\mathrm{M}}(t)) = & -\sum_{\ell\in\Omega_{2+}}\exp\left(\ell(\mathrm{i}\pi/2+\alpha)\right)\left(\exp(-\mathrm{i}\ell B)\left(\frac{\exp(-\alpha)\exp(\mathrm{i}B)-\exp(\alpha)\exp(-\mathrm{i}B)}{\mathrm{i}B-\alpha}\right)\right.\\ & \left.+\exp(\mathrm{i}\ell B)\left(\frac{\exp(\alpha)\exp(\mathrm{i}B)-\exp(-\alpha)\exp(-\mathrm{i}B)}{\mathrm{i}B+\alpha}\right)\right)\\ & -\left(\frac{1-\exp(\alpha-\mathrm{i}B)}{\mathrm{i}B-\alpha}+\frac{\exp(\alpha+\mathrm{i}B)-1}{\mathrm{i}B+\alpha}\right)+C.\end{aligned}\tag{A.6}$$

If we set now

$$\mathcal{N}_\ell(\alpha) = \exp(\mathrm{i}\ell B)\left(\frac{\exp(\alpha)\exp(\mathrm{i}B) - \exp(-\alpha)\exp(-\mathrm{i}B)}{\mathrm{i}B+\alpha}\right),$$
$$\text{and} \quad \mathcal{M}(\alpha) = \frac{\exp(\alpha+\mathrm{i}B)-1}{\mathrm{i}B+\alpha}. \tag{A.7}$$

Then:

$$\mathcal{F}(g_{\mathrm{M}}(t)) = -\sum_{\ell\in\Omega_{2+}} \exp\left(\ell(\mathrm{i}\pi/2+\alpha)\right)(\mathcal{N}_\ell(\alpha)+\mathcal{N}_\ell^*(\alpha)) - (\mathcal{M}(\alpha)+\mathcal{M}(\alpha)^*) + C. \tag{A.8}$$

It is easy to deduce for very small α that

$$\mathcal{M}(\alpha)+\mathcal{M}^*(\alpha) = 2\frac{\sin(t-\pi/2)}{t-\pi/2} + \mathcal{O}(\alpha) \tag{A.9}$$

and that

$$\mathcal{N}_\ell(\alpha)+\mathcal{N}_\ell^*(\alpha) = 4\cos\left(\ell(t-\pi/2)\right)\frac{\sin(t-\pi/2)}{t-\pi/2} + \mathcal{O}(\alpha) \tag{A.10}$$

and then after simplification of the summation by Taylor expansion, we have

$$\mathcal{F}(g_{\mathrm{M}}(t)) = -2\frac{\sin(t-\pi/2)}{t-\pi/2}\left(1+2\sum_{\ell\in\Omega_{2+}}\exp(\ell(\mathrm{i}\pi/2+\alpha))\cos(t-\pi/2) + \mathcal{O}(\alpha)\right) + C. \tag{A.11}$$

We then deduce that this model produces one main centered pulse and residual oscillation taking the modulus of $\mathcal{F}(g_{\mathrm{M}}(t))$.

References

[1] Corkum P B and Krausz F 2007 *Nat. Phys.* **3** 381
[2] Corkum P B 1993 *Phys. Rev. Lett.* **71** 1993
[3] Lewenstein M *et al* 1994 *Phys. Rev.* A **49** 2117
[4] Bandrauk A D, Chelkowski S and Goudreau S 2005 *J. Mod. Opt.* **52** 411
[5] Bandrauk A D, Barmaki S and Lagmago Kamta G 2006 *Progress in Ultrafast Intense Laser Science* vol III ed K Yamanouchi *et al* (Amsterdam: Kluwer)
[6] Lein M 2007 *J. Phys. B: At. Mol. Opt. Phys.* **40** R135
[7] Lagmago Kamta G and Bandrauk A D 2006 *Phys. Rev.* A **74** 033415
[8] Velotta R *et al* 2001 *Phys. Rev. Lett.* **87** 183901
[9] Bandrauk A D, Yu H, Chelkowski S and Constant E 1997 *Phys. Rev.* A **56** 2537
[10] Lan P *et al* 2006 *Phys. Rev.* A **74** 063411
[11] Vozzietal C 1995 *Phys. Rev. Lett.* **95** 153902
[12] Itatani J *et al* 2004 *Nature* **432** 867
[13] Kawai T, Minemote S and Sakai A 2005 *Nature* **435** 470
[14] Bandrauk A D, Barmaki S and Lagmago Kamta G 2007 *Phys. Rev. Lett.* **98** 013001
[15] Cas W *et al* 2006 *Phys. Rev.* A **74** 063821
[16] Yudin G L, Chelkowski S, Bandrauk A D and Corkum P B 2007 *J. Phys. B: At. Mol. Opt. Phys.* **40** F93
[17] Theberge F *et al* 2006 *Phys. Rev. Lett.* **97** 023904
[18] Painter J C *et al* 2006 *Opt. Lett.* **31** 3471
[19] Gaarde M B, Murakami M and Kienberger R 2006 *Phys. Rev.* A **74** 053401
[20] Chelkowski S, Foisy C and Bandrauk A D 1997 *Phys. Rev.* A **57** 1176
[21] Bandrauk A D and Nguyen H S 2002 *Phys. Rev.* A **66** 031401

[22] Nguyen H S and Suda A 1999 *Phys. Rev.* A **60** 2587
[23] Bandrauk A D, Chelkowski S and Nguyen H S 2004 *J. Mol. Struct.* **735C** 203
[24] Lorin E, Chelkowski S and Bandrauk A D 2007 *Comput. Phys. Commun.* **177** 12
[25] Rae S C and Burnett K 1992 *Phys. Rev.* A **46** 1084
[26] Lorin E, Chelkowski S and Bandrauk A D 2007 *AMS/CRM Proceedings and Notes*, 41
[27] Brabec T and Krausz F 1997 *Phys. Rev. Lett.* **78** 3282
[28] Geissler M, Tempea G and Brabec T 2000 *Phys. Rev.* A **62** 033817
[29] Burnett *et al* 1992 *Phys. Rev.* A **45** 3347
[30] Lagmago Kamta G and Bandrauk A D 2005 *Phys. Rev.* A **71** 053407
[31] de Bohan A, Antoine L P, Milosevic D B and Piraux B 1998 *Phys. Rev. Lett.* **81** 13001
[32] Alfano R R 1989 *The Supercontinuum Laser Source* (New York: Springer)
[33] Corkum P B 2007 Private communication